LAWRENCE
LIVERMORE
NATIONAL
LABORATORY

UCRL-JRNL-228470

Analog and Digitgal Simulations of Maxwellian Plasmas for Astrophysics

D. W. Savin, N. R. Badnell, P. Beiersdorfer, B. R. Beck, G. V. Brown, P. Bryans, T. W. Gorczyca, M. F. Gu, S. M. Kahn, J. M. Laming, D. A. Liedahl, W. Mitthumsiri, J. H. Scofield, K. L. Wong

February 28, 2007

Canadian Journal of Physics

Analog and Digital Simulations of Maxwellian Plasmas for Astrophysics

D. W. Savin,[1,*] N. R. Badnell,[2] P. Beiersdorfer,[3] B. R. Beck,[3] G. V. Brown,[3] P. Bryans,[1] T. W. Gorczyca,[4] M. F. Gu,[3] S. M. Kahn,[5] J. M. Laming,[6] D. A. Liedahl,[3] W. Mitthumsiri,[1] J. H. Scofield,[3] and K. L. Wong[3]

[1]*Columbia Astrophysics Laboratory, Columbia University, New York, NY 10027, USA*

[2]*Department of Physics, University of Strathclyde, Glasgow, G4 0NG, UK*

[3]*Lawrence Livermore National Laboratory, Livermore, CA 94550, USA*

[4]*Department of Physics, Western Michigan University, Kalamazoo, MI 49008, USA*

[5]*Kavli Institute for Particle Astrophysics and Cosmology, Stanford Linear Accelerator Center and Stanford University, 2575 Sand Hill Road, Menlo Park, CA 94025*

[6]*E. O. Hulburt Center for Space Research, US Naval Research Laboratory, Code 7674L, Washington, DC 20375, USA*

(Dated: February 7, 2007)

Abstract

Many astrophysical and laboratory plasmas possess Maxwell-Boltzmann (MB) electron energy distributions (EEDs). Interpreting or predicting the properties of these plasmas requires accurate knowledge of atomic processes such as radiative lifetimes, electron impact excitation and de-excitation, electron impact ionization, radiative recombination, dielectronic recombination, and charge transfer for thousands of levels or more. Plasma models cannot include all of the needed levels and atomic data. Hence approximations need to be made to make the models tractable. Here we report on an "analog" technique we have developed for simulating a Maxwellian EED using an electron beam ion trap and review some recent results using this method.

A subset of the atomic data needed for modeling Maxwellian plasmas relates to calculating the ionization balance. Accurate fractional abundance calculations for the different ionization stages of the various elements in the plasma are needed to reliably interpret or predict the properties of the gas. However, much of the atomic data needed for these calculations have not been generated using modern theoretical methods and are often highly suspect. Here we will also review our recent updating of the recommended atomic data for "digital" computer simulations of MB plasmas in collisional ionization equilibrium (CIE), describe the changes relative to previously recommended CIE calculations, and discuss what further recombination and ionization data are needed to improve this latest set of recommended CIE calculations.

PACS numbers: 34.70.+e,34.80.Dp, 34.80.Kw, 34,80,Lx, 52.50.-j, 52.20.Fs, 52.20.Hv, 52.25.Jm, 52,72.+v, 52.75.-d, 95.30.Dr, 95.30.Ky, 98.38.Bn, 98.58.Bz

*Electronic address: savin@astro.columbia.edu

I. MAXWELL-BOLTZMANN (MB) PLASMAS

Plasmas with a Maxwell-Boltzmann (MB) electron energy distribution (EED) are ubiquitous. In the cosmos they are observed in the sun and other stars, supernova remnants, galaxies, and the intercluster medium of clusters of galaxies. In the laboratory MB plasmas are found in fusion devices, Z-pinches, laser produced plasmas, and many other sources.

Interpreting or predicting the properties of MB plasmas is challenging. Atomic data are needed for thousands upon thousands of processes. Experiments can provide only a fraction of the needed data. Theory provides the bulk of the data, but approximations need to be made to keep the calculations tractable. Also, plasma models cannot include all the needed data without becoming computationally prohibitive.

One solution to this problem of understanding MB plasmas is to effectively build an analog computer in the laboratory. This can be done by creating an MB plasma under controlled condition to benchmark plasma models. This tests everything at once, both the plasma model and the underlying atomic data.

Here we report on work which we have carried out over the last decade to improve our understanding of MB plasmas. In Sec. II we describe a method we have developed to use the nearly monoenergetic electron beam in an electron beam ion trap (EBIT) to simulate an MB plasma. This technique was first implemented on the EBIT-II electron beam ion trap at Lawrence Livermore National Laboratory [1] and has recently been adapted to the Livermore EBIT-I device. Our initial tests of the fidelity of the MB simulations are described in Sec. III. Further discussion of our EBIT MB "analog" simulation work is given in Ref. [2].

An important property of steady-state MB plasmas is the collisional ionization equilibrium (CIE) reached in the plasma. In Sec. IV we discuss previous work which has been carried out to calculate fractional ion abundances for astrophysical MB plasmas in CIE. MB studies at the Livermore EBITs have recently been expanded to investigate CIE as noted in Sec. V. Our recent improvements to CIE calculations and some results are presented in Sec. VI. We conclude this paper with discussion of the future atomic data needs for improving our understanding of MB plasmas in CIE. Additional discussion of these "digital" simulations of MB plasmas in CIE are given in Ref. [3].

II. SIMULATING MB PLASMAS IN AN ELECTRON BEAM ION TRAP (EBIT)

A. Simulating an MB energy distribution

The key to simulating a MB plasma using the nearly monoenergetic beam in an EBIT is to sweep the electron beam energy E in time so that

$$\frac{d\tau}{\tau_o} = P(E, T_e)dE \tag{1}$$

where τ_o is the time length of sweep period, τ is the time in this period, and $P(E, T_e)$ is the MB probability at an electron temperature T_e of finding an electron in the energy range E to $E + dE$. Here we have implicitly assumed that the electron density n_e is kept constant. The MB probability is given by

$$P(E, T_e)dE = \frac{2E^{1/2}}{\pi^{1/2}(k_B T_e)^{3/2}} \exp\left(\frac{-E}{k_B T_e}\right) dE \tag{2}$$

where k_B is the Boltzmann constant. As is described in Ref. [2], solving for τ yields

$$\tau(E) = \tau_o \left[\mathrm{erf}(x) - \frac{2xe^{-x^2}}{\sqrt{\pi}}\right], \tag{3}$$

where $\mathrm{erf}(x)$ is the error function, $x = (E/k_B T_e)^{1/2}$, and the quantity in the square brackets ranges between 0 and 1. The electron energy sweep pattern $E(\tau)$ may be calculated numerically using Eq. 3.

B. Maintaining a constant-density electron beam

The electron density is kept constant as E is swept for a number of reasons. This keeps space charge and trapping conditions largely unchanged during the sweeping. It also helps to maintain a constant electron-ion overlap versus beam energy. This last point is important as it helps to ensure all electron-ion collision processes go forward at the correct plasma rates.

The current from a Pierce electron gun, such as is used in the Lawrence EBITs, is given by [4]

$$I_e = pV_a^{3/2}, \tag{4}$$

where p is the perveance in units of amperes volts$^{-3/2}$ and V_a is anode voltage in volts. For a beam with a shape and size constant with E, we have

$$n_e \propto \frac{I_e}{v_e} \propto \frac{V_a^{3/2}}{E^{1/2}}. \tag{5}$$

where v_e is the electron beam velocity at energy E. To keep n_e constant as a function of $E(\tau)$, V_a is swept so that

$$V_a(\tau) = (V_a)_r \left[\frac{E(\tau)}{E_r} \right]^{1/3}, \tag{6}$$

where $(V_a)_r$ is the anode voltage at an arbitrary reference energy E_r.

C. Technical limitations

Technical limitations constrain the implementation of the MB simulation in an EBIT. The most obvious of these are the minimum and maximum energies, E_{min} and E_{max} respectively, between which the beam energy can be swept. For the Livermore EBITs, typically $E_{min} \gtrsim 0.2$ keV. Although measurements can be performed with lower beam energies [5], the electron beam is poorly behaved for these lower energies and does not lend itself to automated control with rapidly varying conditions. This is not expected to be a significant problem for studying X-ray emitting plasmas as most collision processes of interest occur for $E > 0.2$ keV.

Values of E_{max} are typically kept to $\leq (5-6)k_BT_e$. This is due to capacitances limiting dE/dt and dV_a/dt to ≤ 30 V/μs in the Livermore EBIT machines. As a result, the highest energy electrons in the MB distribution are not sampled. These constitute typically $\leq 2\%$ of the total EED.

Due to the E_{min} and E_{max} limitation, we do not sweep over the entire period τ_o. The actual sweep period is given by $t_o = \tau(E_{max}) - \tau(E_{min})$. The specific time versus E in the applied sweep pattern $E(t)$ is given by $t(E) = \tau(E) - \tau(E_{min})$.

To avoid problems of trying to sweep faster than the slew rate of the EBIT electrical system, we sweep from E_{min} to E_{max} and then back down to E_{min} using the same pattern as the upsweep but mirrored around $t = t_o$. For the T_e range we are interested in simulating, the maximum slew rate for E limits t_o to values $\gtrsim 5$ ms.

Additionally, the space charge effects of the electron beam and trapped ions on the actual electron energy in the trap need to be estimated and corrected for (a correction typically on the order of 50-100 V). Lastly, the electron beam energy needs to be swept faster than the time scale over which the collision processes of interest occur. This is necessary in order to insure that the trapped ions see an actual MB EED (albeit a time-averaged one). Typical sweep times are on the order of 5 ms.

D. Representative sweep patterns

Figure 1 shows the sweeping pattern used to simulate an MB plasma of $k_B T_e = 2.4$ keV. Operating conditions were used with $E_{min} = 0.6$ keV, $E_{max} = 12.24$ keV, $(V_a)_{min} = 1.2$ kV, and $t_o = 5$ ms. The sweep patterns rises smoothly up from E_{min} to E_{max} and smoothly back down to E_{min}. We avoid jumping from E_{max} immediately back down to E_{min} because of the limited slew rates for E and V_a described above. Figure 2 shows the derivatives of the slew rates plotted in Fig. 1. E_{max} has been chosen to keep $dE/dt < 30$ V μs^{-1}.

III. FIDELITY OF THE MB SIMULATIONS

To verify the accuracy of our simulated MB EEDs, we have carried out measurements of line emission due to dielectric recombination (DR) and electron impact excitation (EIE) of heliumlike neon, magnesium, and argon. Heliumlike ions are commonly used to measure the electron temperature of a plasma by taking the ratio of DR produced lines to EIE lines [6].

Figure 3 shows pictorially how we were able to test the fidelity of the simulated MB EED. The ratio of line emission due to the DR resonance line known as j relative to the electron impact excitation line known as w can be used as a temperature diagnostic. Here we use the notation of Ref. [7]. The j line samples the EED at a single energy while w integrates the EED from the EIE threshold and up. As the temperature changes, so do the portions of the MB EED sampled. Thus, as the temperature of the plasma changes, the j/w ratio correspondingly changes [6].

A representative scatter plot of MB data take on EBIT-II is shown in Fig. 4 for Mg^{10+} at a simulated temperature of $k_B T_e = 0.7$ keV. Extracting the integrated line intensities for j and w for a number of different simulated temperatures yields data such as that shown in Fig. 5. We can then turn around and use the experimental and theoretical data shown in Fig. 5 to infer the MB temperature based on the measured j/w ratio and the range of theoretical predictions for this ratio. Figure 6 shows the resulting spectroscopically inferred temperature versus the simulated temperature at which the data were collected. Lastly, Fig. 7 replots these data to further emphasize the excellent EED fidelity we are able to achieve in our EBIT MB simulations.

IV. COLLISIONAL IONIZATION EQUILIBRIUM (CIE) CALCULATIONS

CIE occurs in plasma which are optically thin to radiation, of low enough density that three-body recombination is unimportant, dust-free so recombination on grains is not an issue, and in steady state or nearly so. Under these conditions the electron impact ionization (EII) rate equals the electron-ion recombination rate. Hence the accuracy of these rates determines reliability of the fraction ionic abundances calculated by a CIE model.

In astrophysics, plasmas in CIE are found in the Sun and other stars, galaxies, and the intercluster medium. An early set of CIE calculations for astrophysical modeling are those of Shull and van Steenberg [8] who compiled published DR, radiative recombination (RR), and EII data. These data were updated by Arnaud and Rothenflug [9] and then again by Arnaud and Raymond [10] specifically for iron. Subsequently Mazzotta et al. [11] re-evaluated and updated the recombination data used in the models. Most recently we have updated the recombination data using state-of-the-art theoretical DR and RR results for all K-shell, L-shell, and Na-like ions of H through Zn [3]. Our results are discussed in more detail below.

V. CIE MEASUREMENTS USING EBIT MB SIMULATIONS

EBIT MB simulations can be used to make studies of the ionic abundances, and thus of CIE, as a function of electron temperature. Such measurements have been carried out recently at Livermore to measure the charge state distribution of highly charged gold under CIE conditions [12, 13]. A detailed review of these measurements is given by May et al. in these proceedings.

An important aspect of using an EBIT MB simulation to study CIE is to account for the effect of charge exchange (CX) on the ionic abundances. CX involves collisions between ions and neutrals where an electron is captured by the ion from the neutral.

Although the ions in EBIT are trapped by the space charge of the electron beam, the ions leave the immediate confines of the electron beam and can spend a rather large fraction of the time outside the beam. In fact, this ion-beam overlap has been inferred in several ways and may vary between a few percent to near unity [14, 15]. While outside the beam, the ions are subject to interacting with rest gas neutrals and thus to CX. In that case the

recombination rate may be much larger than that due to the DR and RR rates assumed in CIE. An EBIT MB simulation can thus only be used to reliably study ionic abundances in CIE, if contributions from CX are either minimize and suppressed or accurately known.

In order to test for the effect of CX on the charge state distribution of gold measured with an MB simulation, measurements were made with different concentrations of background gas. In particular, we varied the amount of argon gas injected into the trap using a gas injector with a precisely controlled continuous flow. The absolute value of the neutral gas density n_0 in the trap is unknown. Also, the actual temperature of the ions and thus their velocity v_i is typically unknown, unless special efforts are made to measure it by very high-resolution crystal spectroscopy [16, 17]. However, a way to measure the product of these two parameters has been devised based on operating an EBIT in the so-called magnetic mode [18], which can be used to detect and account for the presence of CX on the CIE.

In the magnetic mode, the x-ray signal induced by the CX decays exponentially as the ions recombine [18]. The exponential decay constant is given by

$$R_{CX} = n_0 v_i \sigma_{CX} \tag{7}$$

where σ_{CX} is the CX cross section of neutral argon with highly charged gold ions. The neutral gas velocity is assumed negligible compared to the velocity of the trapped ions. Fitting the exponential decay of the x-ray signal during the magnetic mode yields R_{CX}. We then plot the average ionic charge state inferred during the MB simulation, i.e., when the electron beam is on, as a function of R_{CX}. The result is shown in Fig. 8. By interpolating the measurements to a value of $R_{CX} = 0$, the MB simulations yield the average ionic abundance in CIE.

For the particular measurement of gold at a simulated temperature of 2.5 keV shown in Fig. 8, the average ionic charge state did not depend on CX. This result is, however, atypical and may be due to the dominance of dielectronic recombination in this case. In typical situations, the CX recombination rate exceeds that due to RR by factors of five [19].

VI. NEW THEORETICAL CIE RESULTS

In the past 4 years there have been significant theoretical advances in the DR and RR data available for modeling cosmic plasmas (as discussed in Ref. [3]). Modern DR and RR

calculations have now been carried out by several different groups for K-shell, L-shell, and Na-like ions of all elements from hydrogen up to and including zinc. For a given ion of a given element, these theoretical calculations typically agree with one another to within 25% at the temperatures where that ion forms in CIE. This formation zone is defined here as the temperature range where the fractional ionic abundance is $\geq 1\%$ of the total elemental abundance.

Laboratory measurements have been used to benchmark modern DR calculations. K-shell ions have been well studied using EBITs and ion storage rings. The agreement between theory and experiment is generally within $\sim 20\%$ [20, 21]. L-shell ions are less well studied and the agreement between theory and experiment is $\sim 35\%$ [3, 22, 23]. But as discussed below, additional studies are needed. Additionally, DR theory is much less reliable at $\sim 10^4$ K ($k_B T_e \sim 1$ eV). This is because for the DR resonances important in 10^4 K plasmas, the uncertainties in the theoretical resonance energies can be comparable to the resonance energy. This results in a large uncertainty in the calculated DR rate coefficient. Barring theoretical advances in this area, laboratory measurements remain the only reliable way to produce the DR data needed for ions forming at these temperatures.

We have incorporated these new DR and RR rate coefficients into our CIE models [3]. Our results differ significantly from the CIE results of Mazzotta et al. [11] which were the previous state-of-the-art for CIE calculations in astrophysics. We find peak fractional abundances which differ by up to 60%. At fractional abundances of 0.1, we find differences of up to a factor of 5. At 0.01, this can increase up to a factor of 11. The peak formation temperature for an ion can shift by up to 20%. Ions with particularly large differences include Mg, Al, Ca, Fe, Co, and Ni.

Figure 9 shows a comparison between our calculated CIE fractional abundances for iron and those of Mazzotta et al. Here we have used recently published AUTOSTRUCTURE calculations for DR [24] and RR [25]. Note that no significant differences between our results and those of Mazzotta et al. are seen for charge states much lower than sodiumlike. This is because the DR and RR data have been updated only for sodiumlike ions and more highly ionized charge states.

We have also carried out CIE calculations using the FAC DR and RR data of Ref. [26–28]. These results are in good agreement the the AUTOSTRUCTURE-based CIE results. We find that the peak fractional abundance differs by $\leq 10\%$. At 0.1 fractional abundances,

differences are $\leq$ 30%, and at 0.01 they are $\leq$ 50%. This good agreement reflects the good agreement between the AUTOSTRUCTURE and FAC DR and RR data. Figure 10 shows a comparison between the AUTOSTRUCTURE-based and FAC-based CIE fractional abundances for iron.

VII. FUTURE MODELING NEEDS FOR MB PLASMAS IN CIE

A significant amount of recombination and ionization data are needed to improve CIE models for astrophysics. We discuss these needs in detail in Ref. [3]. Our comments here refer to ions of elements from hydrogen up to and including zinc.

For RR, theoretical and experimental data are needed for M-shell ions of elements up to and including zinc. For DR of L-shell ions, laboratory measurements are needed for boronlike, carbonlike, nitrogenlike, oxygenlike, fluorinelike, and neonlike ions. Modern theoretical calculations exist for these isoelectronic sequences but there is a paucity of laboratory studies to benchmark the theory. Additionally, as discussed above, the reliability of DR theory at temperatures of $\sim 10^4$ K is poor and laboratory data are needed for ions forming at these temperatures. More accurate atomic structure codes could remove much of the uncertainties in the DR theory. More importantly is the lack of DR for ions with partially filled M-shells. Initial theoretical and experimental work has been carried out for M-shell iron ions [29–31], but significant work remains.

The EII data base used in astrophysics has essentially remained unchanged for almost 20 years. An excellent review of the status of the EII data base is given in Ref. [32]. In that review, the authors found factor of $2-3$ difference between various recommended published EII data sets (e.g., [9, 33]). This is rather surprising as the published data sets all make use of the same few theoretical and experimental results.

An updating of the EII database is sorely needed. Much of the existing data are based on experiments with unknown metastable fractions. The recommended EII data used in astrophysics has not been updated since around 1990. This is partly because few new laboratory measurements or theoretical calculations exist.

CX is both a recombination and an ionization process and is most important for near-neutral systems (charge ≤ 4) [9]. In astrophysics CX with H is important at temperatures $\lesssim 25,000$ K [3]. CX in CIE has been investigated in Ref. [9]. These data need to be updated

to reflect recent advances and incorporated into CIE models.

It is clear that vast quantities of data are still needed for reliable CIE models for astrophysics. We propose that these data should be generated with an accuracy of 35% or better. This is the level of accuracy for the recent state-of-the-art DR and RR calculations and measurements. It would be good if the remaining needed recombination and ionization data were at the same level of accuracy. Additionally, EBIT MB simulations would be quite helpful in testing the current generation of CIE models.

Acknowledgments

Work at Columbia University was supported in part by a NASA Solar and Heliospheric Physics Supporting Research and Technology grant and an NSF Division of Astronomical Sciences Astronomy and Astrophysics Research grant. Work at Lawrence Livermore National Laboratory (LLNL) and Stanford University was supported in part by a NASA Astronomy and Physics Research and Analysis grant. Work at the University of California LLNL was performed uner the auspices of the U.S. Department of Energy under Contract No. W-7405-Eng-48.

[1] D. W. Savin, B. Beck, P. Beiersdorfer, S. M. Kahn, G. V. Brown, M. F. Gu, D. A. Liedahl, and J. H. Scofield, Physica Scripta **T80**, 312 (1999).

[2] D. W. Savin, P. Beiersdorfer, S. M. Kahn, B. R. Beck, G. V. Brown, M. F. Gu, D. A. Liedahl, and J. H. Scofield, Rev. Sci. Instrum. **71**, 3362 (2000).

[3] P. Bryans, N. R. Badnell, T. W. Gorczyca, J. M. Laming, W. Mitthumsiri, and D. W. Savin, Astrophys. J. Suppl. Ser. **167**, 343 (2006).

[4] G. R. Brewer, in *Focusing of Charged Particles*, ed. by A. Septier (Academic Press, New York, 1967), 23.

[5] J. K. Lepson and P. Beiersdorfer, Physica Scripta T120, 62 (2005).

[6] J. Dubau and S. Volonté, Rep. Prog. Phys. **43**, 199 (1980).

[7] A. H. Gabriel, Mon. Not. R. Astron. Soc. **160**, 99 (1972).

[8] J. M. Shull and M. van Steenberg, Astrophys. J. Suppl. Ser. **48**, 95 (1982); erratum **49**, 351 (1982).

[9] M. Arnaud and R. Rothenflug, Astron. Astrophys. Suppl. Ser. **60**, 425 (1985).

[10] M. Arnaud and J. C. Raymond, Astrophys. J. **398**, 394 (1992).

[11] P. Mazzotta, G. Mazzitelli, S. Colafrancesco, and N. Vittorio, Astron. Astrophys. Suppl. Ser. **133**, 403 (1998).

[12] K. L. Wong, M. J. May, P. Beiersdorfer, K. B. Fournier, B. Wilson, G. V. Brown, P. Springer, P. A. Neill, and C. L Harris, Phys. Rev. Lett. **90**, 235001 (2003).

[13] M. J. May, P. Beiersdorfer, M. Schneider, S. Terracol, K. L. Wong, K. Fournier, B. Wilson, J. H. Scofield, K. J. Reed, G. Brown, F. S. Porter, R. Kelley, C. A. Kilbourne, and K. P Boyce, in *CP370 Atomic Processes in Plasmas: 14th APS Topical Conference on Atomic Processes in Plasmas*, edited by J. S. Cohen, S. Mazevet, and D. P. Kilcrease (American Institute of Physics, Melville, New York, 2004), p. 61

[14] K. L. Wong, P. Beiersdorfer, R. E. Marrs, B. M. Penetrante, K. J. Reed, J. H. Scofield, D. A. Vogel, and R. Zasadzinski, Nucl. Instrum. Methods **B72**, 234 (1992).

[15] D. R. Dewitt, D. Schneider, M. W. Clark, M. H. Chen, and D. Church, Phys. Rev. A **44**, 7185 (1991).

[16] P. Beiersdorfer, V. Decaux, S. R. Elliott, K. Widmann and K. Wong, Rev. Sci. Instrum. **66**,

303 (1995).

[17] P. Beiersdorfer, V. Decaux, and K. Widmann, Nucl. Instrum. Methods **B98**, 566 (1995).

[18] P. Beiersdorfer, L. Schweikhard, J. Crespo López-Urrutia, and K. Widmann, Rev. Sci. Instrum. **67**, 3818 (1996).

[19] P. Beiersdorfer, A. L. Osterheld, M. H. Chen , J. R. Henderson, D. A. Knapp, M. A. Levine, R. E. Marrs, K. J. Reed, M. B. Schneider, and D. A. Vogel, Phys. Rev. Lett. **65**, 1995 (1990).

[20] A. Müller, in Atomic and Plasma-Material Interaction Data for Fusion, Suppl. to Nucl. Fusion, Vol. 6 (International Atomic Energy Agency, Vienna, 1995), p. 59.

[21] D. W. Savin and J. M. Laming, Astrophys. J. **566**, 1166 (2002).

[22] S. Schippers, Physica Scripta **80**, 158.

[23] D. W. Savin, G. Gwinner, M. Grieser, R. Repnow, M. Schnell, D. Schwalm, A. Wolf, S.-G. Zhou, S. Kieslich, A. Müller, S. Schippers, J. Colgan, S. D. Loch, N. R. Badnell, M. H. Chen, and M. F. Gu, Astrophys. J. **642**, 1275 (2006).

[24] N. R. Badnell, M. G. O'Mullane, H. P. Summers, Z. Altun, M. A. Bautista, J. Colgan, T. W. Gorczyca, D. M. Mitnik, M. S. Pindzola, and O. Zatsarinny, Astron. Astrophys. **406**, 1151 (2003); http://amdpp.phys.strath.ac.uk/tamoc/DR.

[25] N. R. Badnell, Astophys. J. Suppl. Ser. **167**, 334 (2006); http://amdpp.phys.strath.ac.uk/tamoc/RR

[26] M. F. Gu, Astrophys. J. **590**, 1131 (2003).

[27] M. F. Gu, Astrophys. J. Suppl. Ser. **153**, 389 (2004).

[28] M. F. Gu, Astrophys. J. **589**, 1085 (2003).

[29] E. W. Schmidt, S. Schippers, A. Müller, M. Lestinsky, F. Sprenger, M. Grieser, R. Repnow, A. Wolf, C. Brandau, D. Lukić, M Schnell, and D. W. Savin, Astrophys. J. Lett. **641**, L157 (2006).

[30] N. R. Badnell, J. Phys. B **39**, 4825 (2006).

[31] N. R. Badnell, Astrophys. J. **651**, L73 (2006).

[32] T. Kato, K. Masai, and M. Arnaud, "Comparison of Ionization Rate Coefficients of Ions from Hydrogen through Nickel," *National Institute for Fusion Science Report, Nagoya, Japan, NIFA-DATA-14* (1991).

[33] M. A. Lennon, K. L. Bell, H. B. Gilbody, J. G. Hughes, A. E. Kingston, M. J. Murray, and F. J. Smith, J. Chem. Phys. Ref. Data **17**, 1285 (1988).

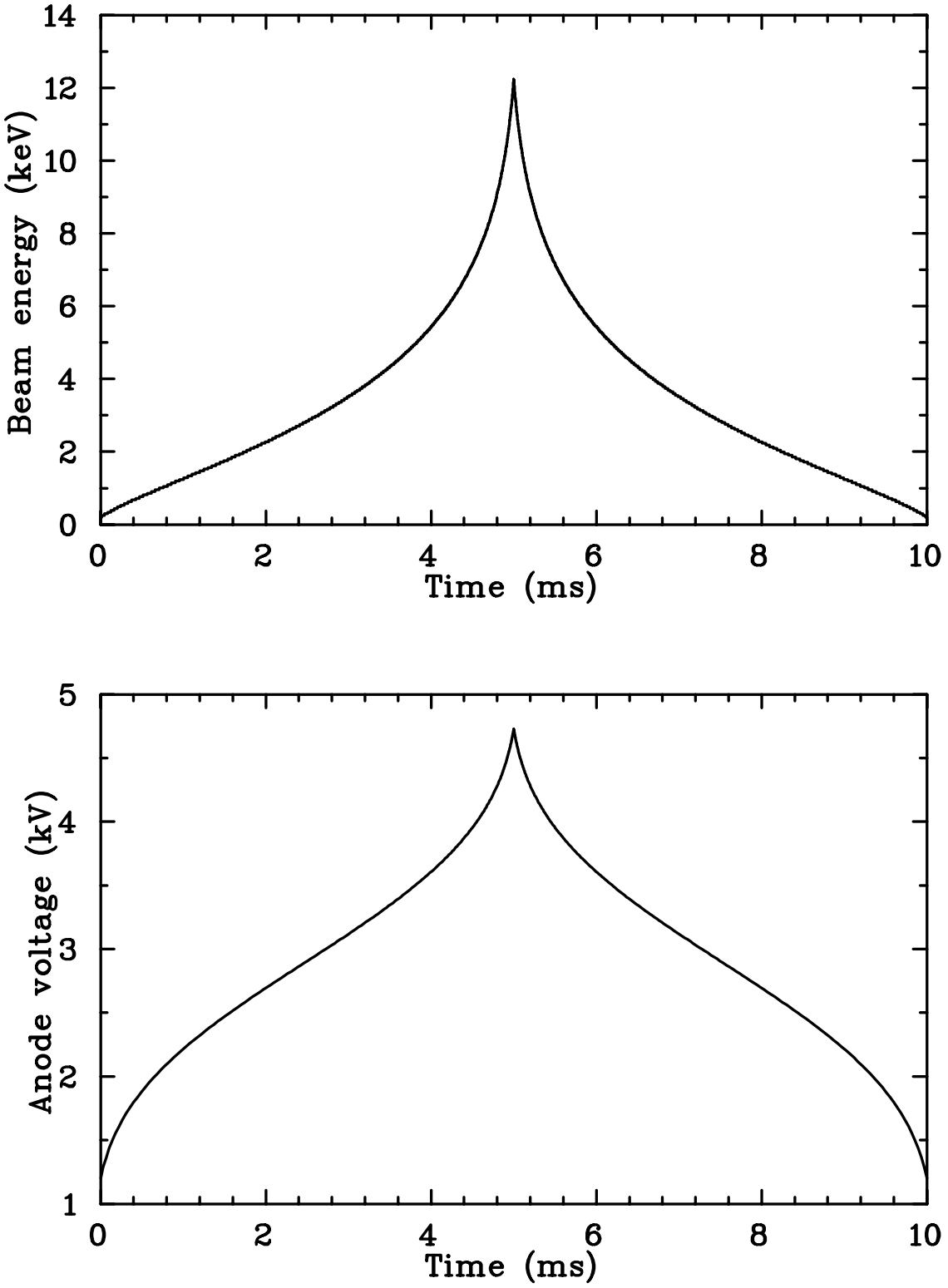

FIG. 1: Digitized timing pattern of the electron beam energy (top) and of the electron gun anode voltage (bottom) used for simulating a Maxwellian plasma at $k_B T_e = 2.4$ keV. Representative operating conditions of $E_{min} = 0.6$ keV, $E_{max} = 12.24$ keV, $(V_a)_{min} = 1.2$ kV, and $t_o = 5$ ms have been used.

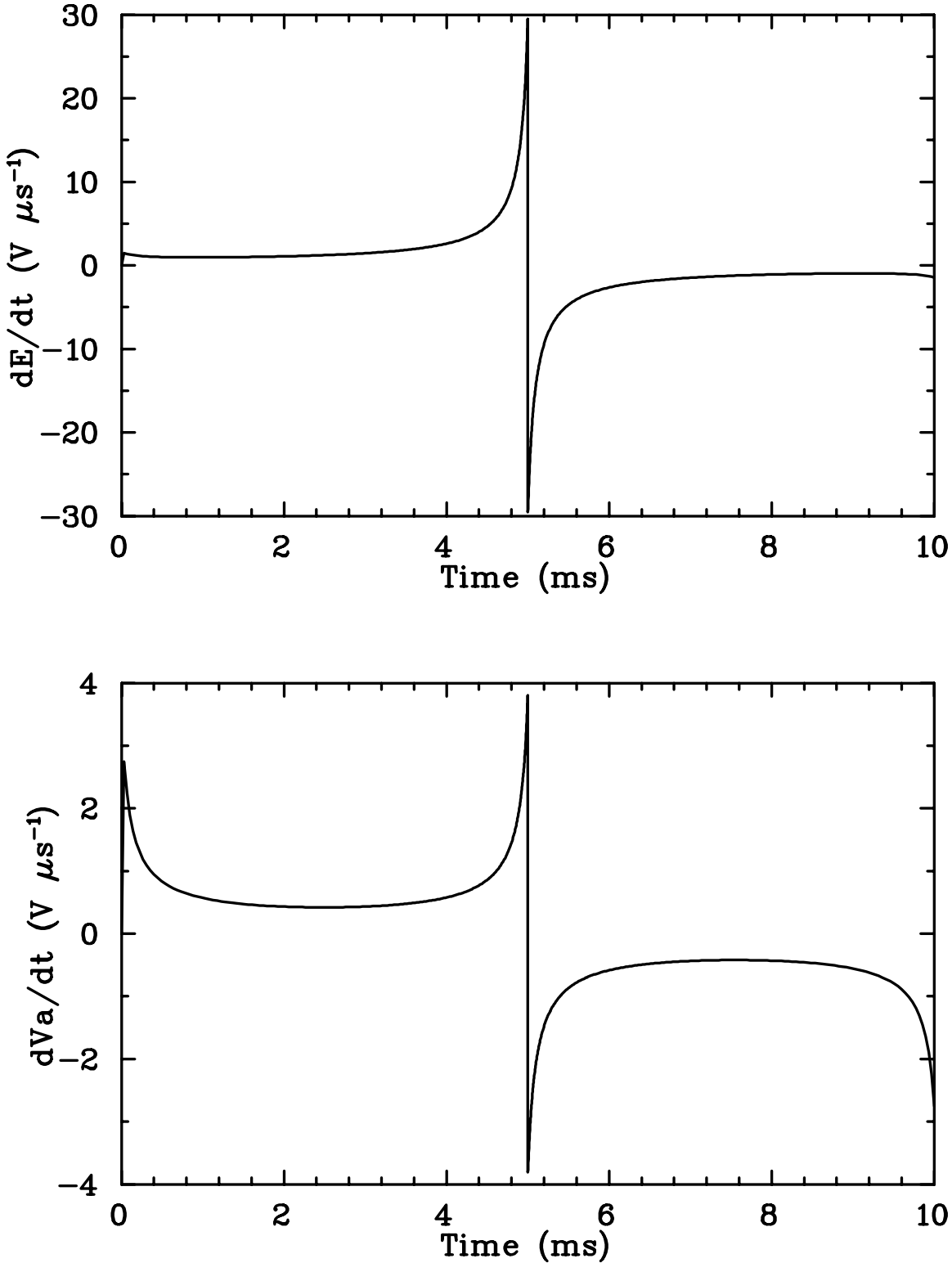

FIG. 2: Derivatives of the timing patterns shown in Fig. 1

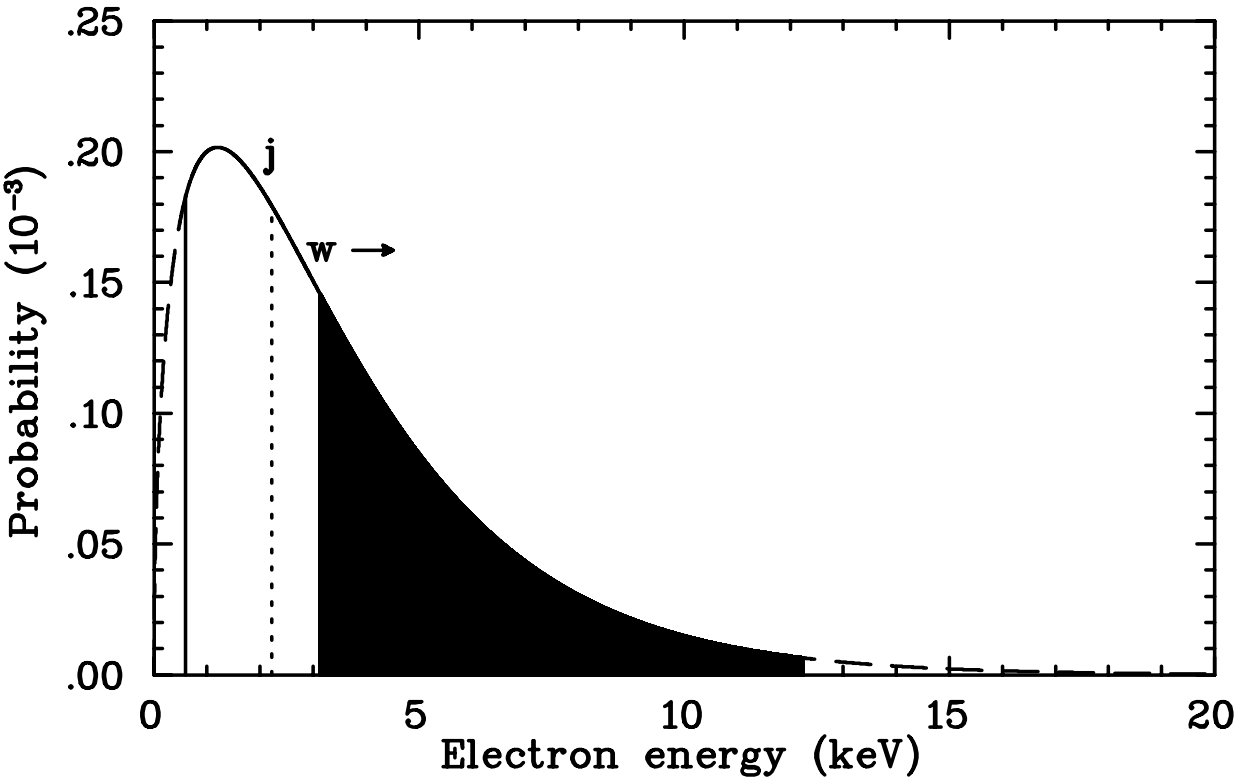

FIG. 3: The *dashed curve* shows a Maxwell-Boltzmann electron energy distribution for $k_B T_e$ = 2.4 keV. The *solid curve* shows the electron energy which is swept out in the simulation generated using the pattern shown in Fig. 1. The *vertical dotted line* shows the electrons contributing to the resonance line labeled as j which is due to DR onto heliumlike ions. The *filled area* under the curve shows the electrons contributing to EIE of w which is the resonance line of heliumlike ions. The ratio of line emission due to j and w is temperature sensitive. See text and Ref. [2] for additional details.

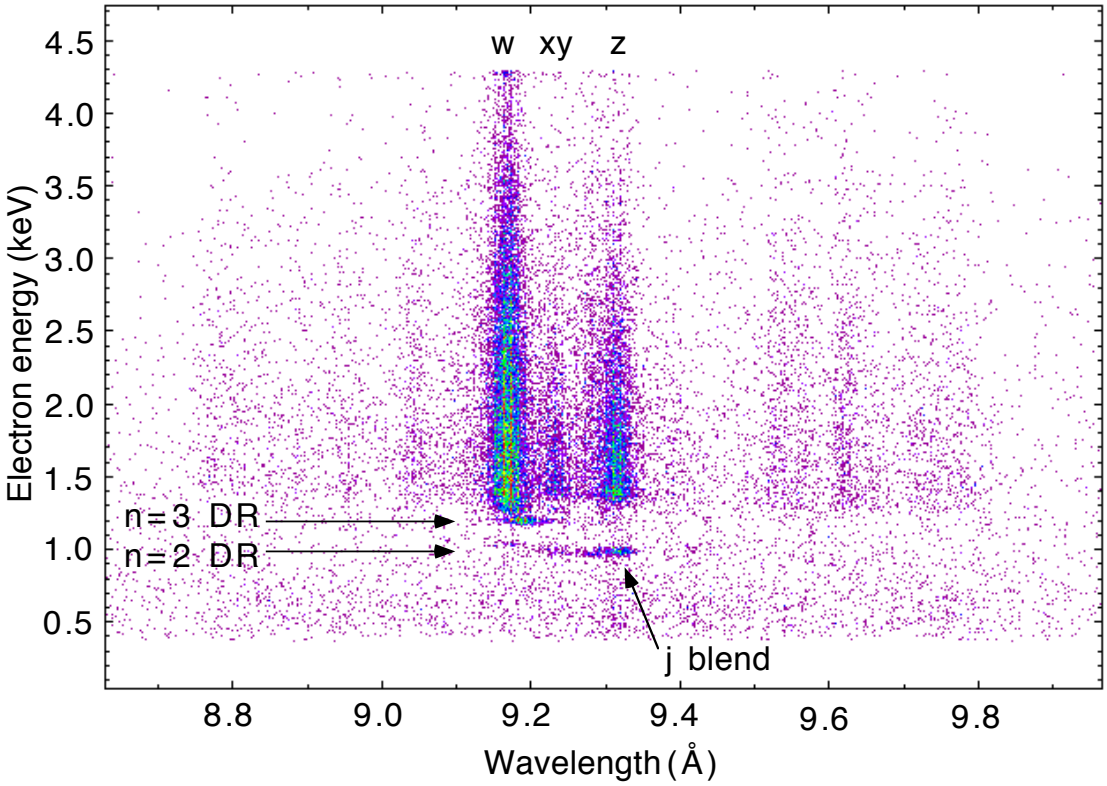

FIG. 4: Scatter plot of photon wavelength versus electron beam energy for an MB simulation of $k_B T_e = 0.7$ keV. The vertical features above $E \sim 1.35$ keV are due to EIE of Mg^{10+} and are (using the notation of Ref. [7]) w, x and y which are blended, and z. The features at $E \sim 0.98$ keV are due to DR into the $n = 2$ level of Mg^{9+}. The features at $E \sim 1.2$ keV are DR into the $n = 3$ level. The tail on w below the EIE threshold energy is due to $n \geq 4$ DR.

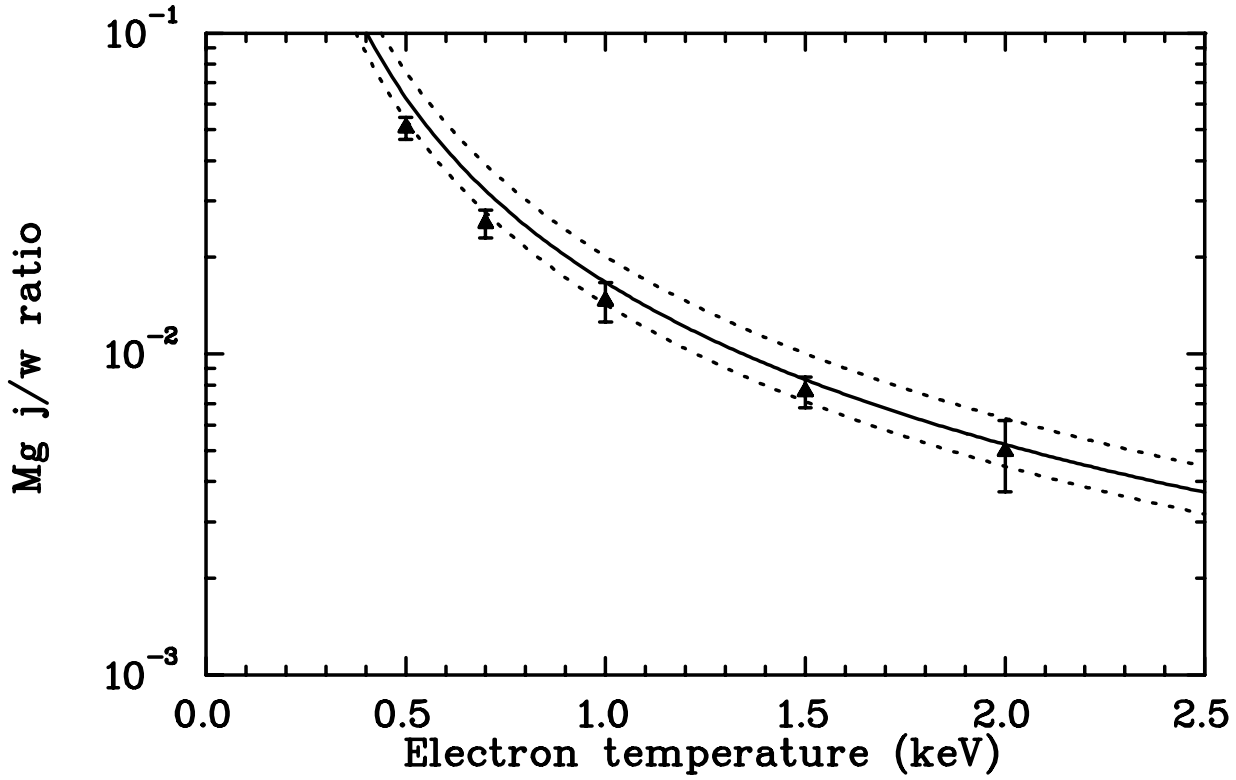

FIG. 5: Measures and theoretical j/w line ratio versus $k_B T_e$ for magnesium. Experimental results are shown with their estimated 1σ confidence limits. The solid curve is the best-guess theoretical line ratio. The dotted curves show the estimated range of the theoretical ratios. These dotted curves represent not 1σ values but rather the maximum and minimum values based on the theoretical results in the literature.

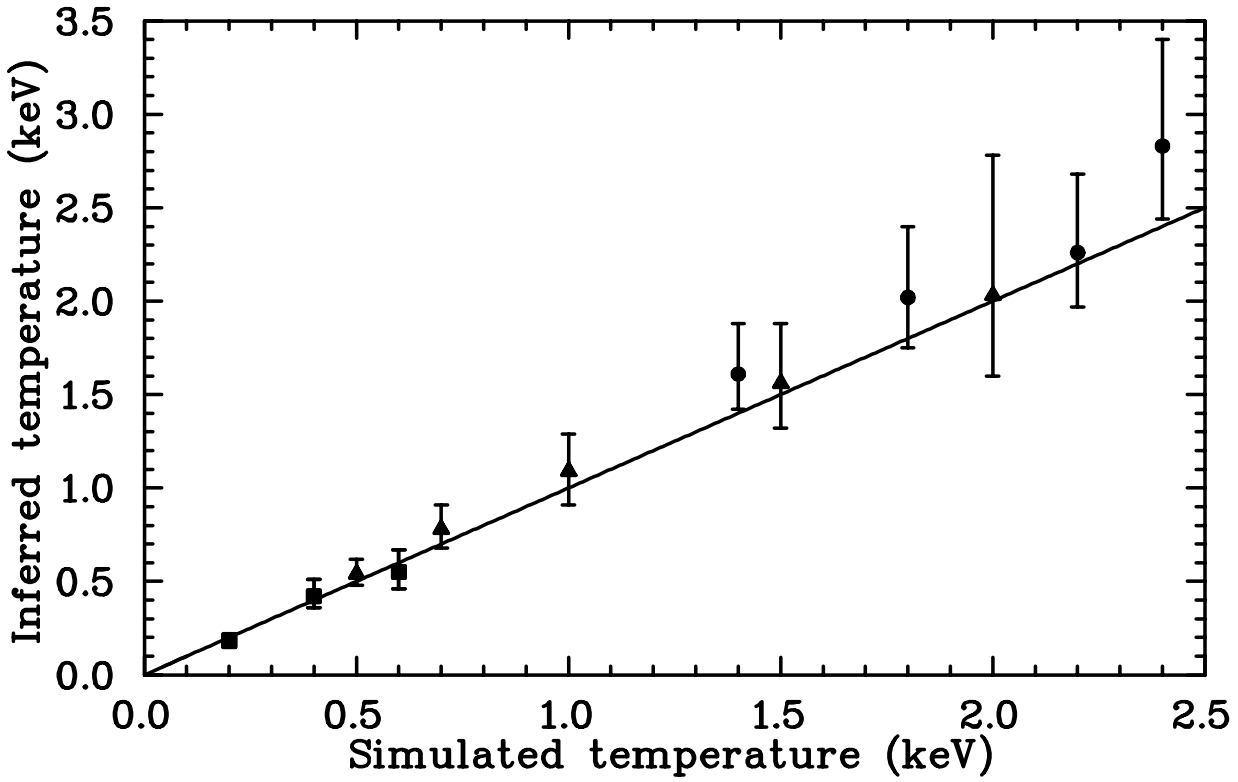

FIG. 6: Spectroscopically inferred $k_B T_e$ (using j/w) plotted as a function of the simulated MB temperature. Data are shown for neon (*circles*), magnesium (*triangles*), and argon (*circles*). The error bars represent the combined effects of the 1σ experimental uncertainties and the range of theoretical j/w ratios. The straight line shows where the inferred and simulated temperatures are equal.

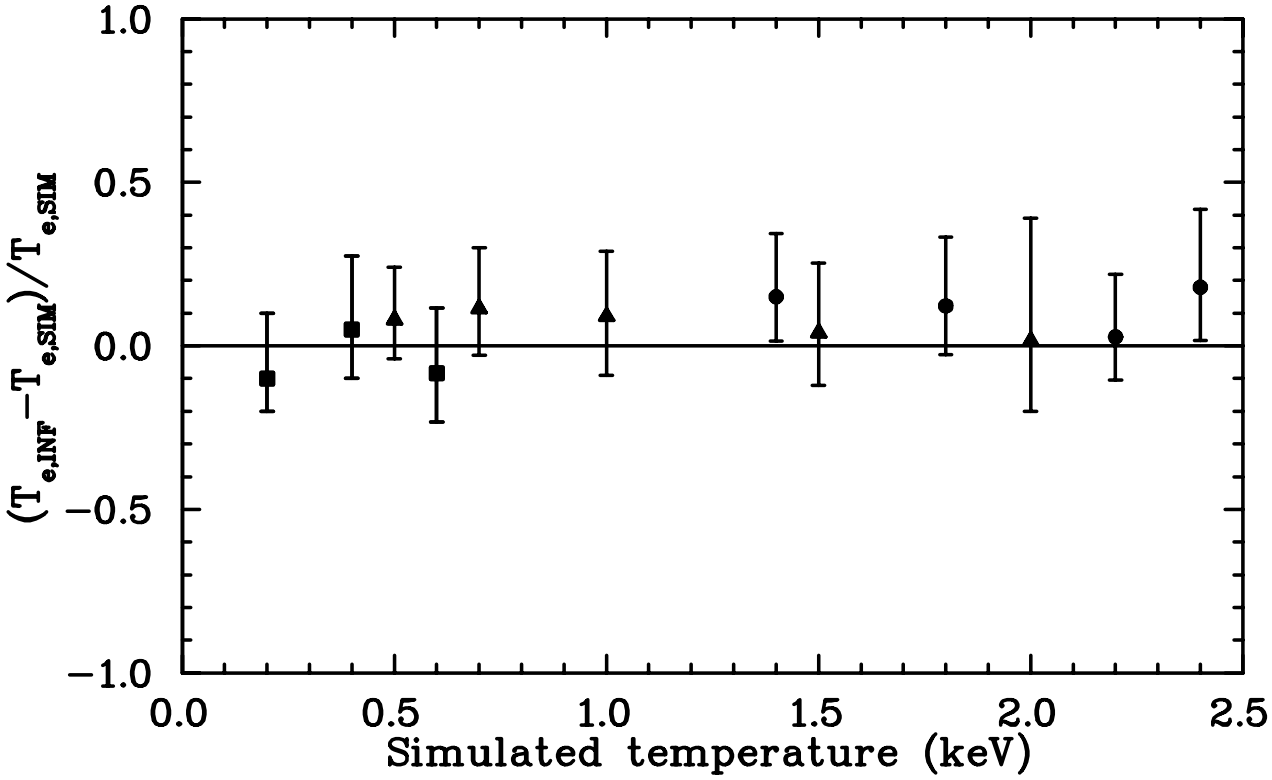

FIG. 7: Fidelity of our simulated MB plasmas using the results from Fig. 6. The ratio is shown for the difference between the simulated and interred temperatures relative to the simulated value. The symbols have the same meaning as in Fig. 6

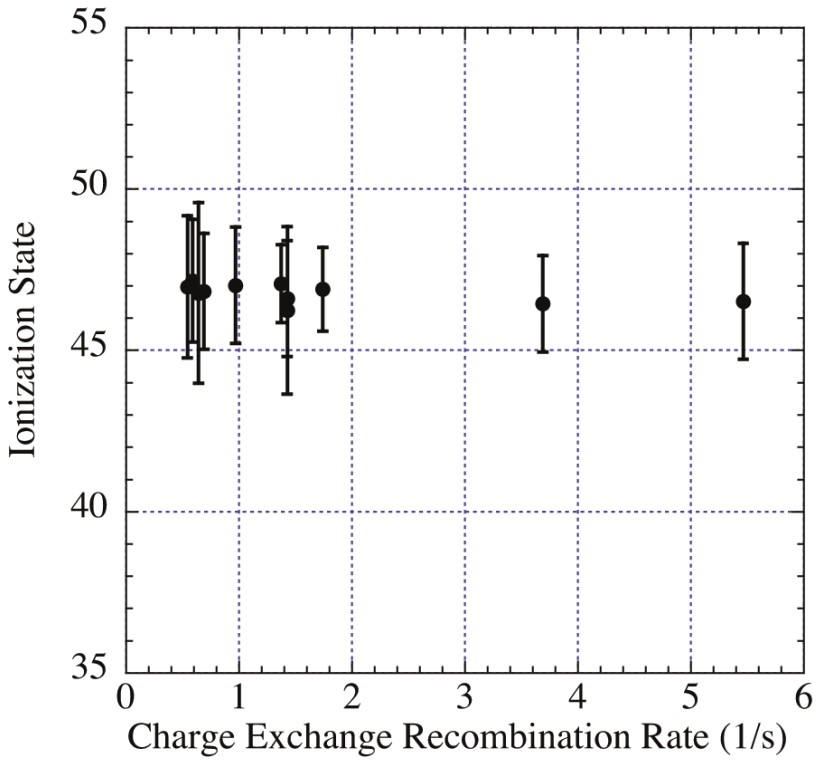

FIG. 8: Average ionic charge of gold for an MB simulation of a 2.5 keV plasma versus the CX rate, R_{CX}.

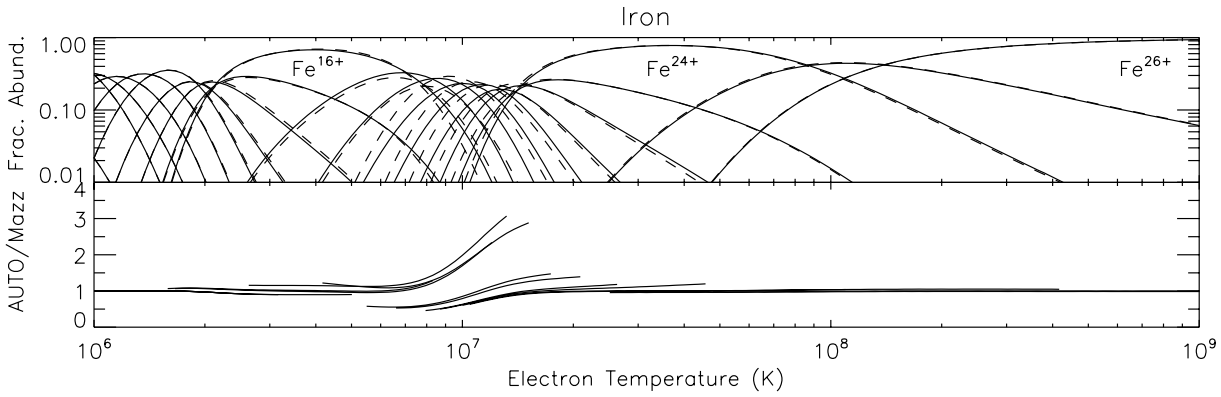

FIG. 9: AUTOSTRUCTURE-based CIE results for iron. The solid curves of the upper graph show the ionization fractional abundance as calculated using the AUTOSTRUCTURE DR rate coefficients of Ref. [24] for hydrogenlike through sodiumlike ions and the AUTOSTRUCTURE RR rate coefficients of Ref. [25] for bare through sodiumlike ions. We use the DR and RR rate coefficients of Mazzotta et al. [11] for ions not calculated in Refs. [24] and [25]. The EII rate coefficients used are those of Ref. [11]. The dashed curves show the abundances calculated by Mazzotta et al. [11]. The lower graph shows the ratio of the calculated abundances. The lowest ionization stage shown is P-like. Comparison is made only for fractional abundances greater than 10^{-2}. We label the AUTOSTRUCTURE-based results as "AUTO" and those of Mazzotta et al. as "Mazz".

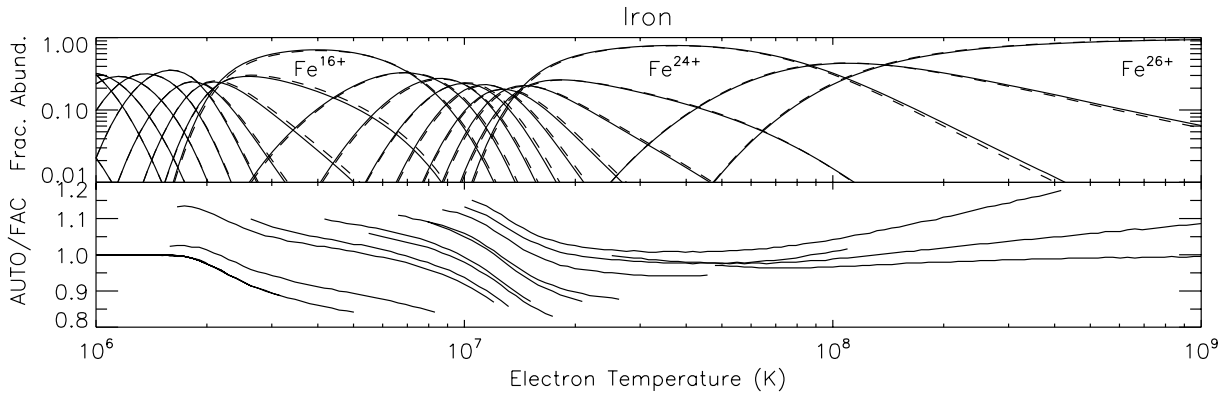

FIG. 10: Comparison with the FAC-based CIE results for iron. The solid curves of the upper graph show the ionization fractional abundance as calculated using the AUTOSTRUCTURE DR rate coefficients of Ref. [24] for hydrogenlike through sodiumlike ions and the AUTOSTRUCTURE RR rate coefficients of Ref. [25] for bare through sodiumlike ions. The dashed curves show the abundances as calculated using the FAC DR rate coefficients of Refs. [26] and [27] for hydrogenlike through sodiumlike ions and the FAC RR rate coefficients of Ref. [28] for bare through fluorinelike ions. We use the DR and RR rate coefficients of Ref. [11] for ions not calculated in Refs. [24–28]. The EII rate coefficients used are those of Ref. [11]. The lower graph shows the ratio of the calculated abundances. The lowest ionization stage shown is P-like. Comparison is made only for fractional abundances greater than 10^{-2}. We label the AUTOSTRUCTURE-based results as "AUTO" and the FAC-based results as "FAC".